Nuclear Physics B356 (1991) 27–45
North-Holland

RENORMALISATION GROUP FLOW IN QED – AN INVESTIGATION OF THE SCHWINGER–DYSON EQUATIONS

P.E.L. RAKOW*

Deutsches Elektronen-Synchrotron DESY, Notkestraße 85, D-2000 Hamburg 52, Germany

Received 27 March 1990
(Revised 16 January 1991)

In this paper I investigate the behaviour of strongly coupled QED using a set of truncated Schwinger–Dyson equations which include the effects of vacuum polarisation. I pay particular attention to the renormalisation group flow. The model has a second-order chiral phase transition, but the renormalised photon coupling α_r is zero at the critical point. I also examine the effects of adding a four-fermion interaction, and find that even with this extra term the photon decouples at the phase transition.

1. Introduction

There has recently been considerable interest in the chiral phase transition of QED [1–5,8–11]. This began when Miransky [1] investigated a truncated Schwinger–Dyson equation for the fermion propagator and found a second-order chiral phase transition, with chiral symmetry spontaneously broken for $\alpha > \pi/3$. Numerous lattice studies [3–5] confirm that non-compact lattice QED has such a phase transition, both in the quenched case and with a low number of dynamical fermion flavours. The interest in this phase transition arose from the suggestion that it might give a non-trivial continuum limit for QED, avoiding the problems (such as the Landau pole [6]) that have previously complicated our understanding of QED.

The Schwinger–Dyson equation which Miransky wrote down did not include any vacuum polarisation effects, using instead the bare photon propagator throughout. It is however very important to include vacuum polarisation when considering the possible triviality of QED, because it is the running of the renormalised charge which leads to problems when attempts are made to take the ultraviolet cut-off Λ to infinity in a theory that is not asymptotically free.

In this paper I investigate a set of Schwinger–Dyson equations that includes the effects of fermion loops on the photon propagator. I find that there is still a

* Present address: Freie Universität Berlin, Institut für Theoretische Physik, Arnimallee 14, D-1000 Berlin 33, Germany.

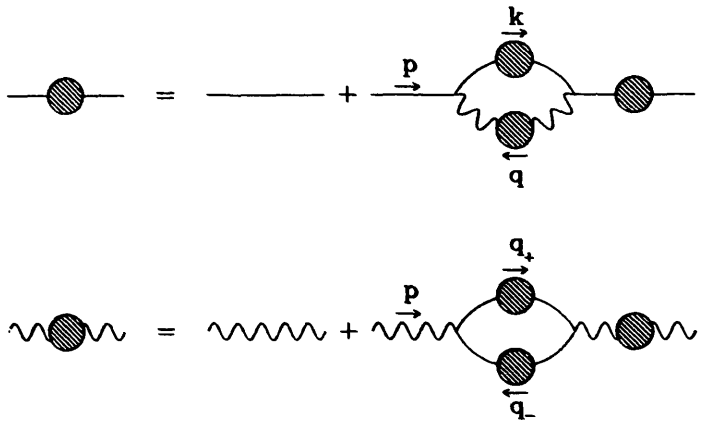

Fig. 1. The Feynman diagrams that lead to the Schwinger–Dyson equations for the fermion and photon propagators.

second-order chiral phase transition, but that the renormalised charge at this transition is zero.

In addition to the renormalised charge I consider the fermion–antifermion scattering amplitude (as Leung, et al. [8] did in the quenched case). These scattering amplitudes show that there are no lines of constant physics in the strong coupling phase of QED, because the scattering amplitudes vary along the lines of constant α_r. Only when an extra interaction is added to the action of QED is it possible to define true renormalisation group trajectories. In sect. 5 I investigate the theory with a chirally invariant four-fermion interaction added, and find that even in this case the renormalised charge at the phase transition is zero.

2. The truncated Schwinger–Dyson equations

In order to study the behaviour of QED in the neighbourhood of the chiral phase transition, where correlation lengths are very large, I derive a set of integral equations for the fermion and photon propagators from the truncated Schwinger–Dyson equations shown in fig. 1. Using the full photon propagator, instead of the bare propagator that Miransky [1] used is an important improvement. This is because it is the vacuum polarisation diagrams, neglected in Miransky's integral equations, which are responsible for the running of the charge in QED. The fermion loops cause the physical coupling at large distance to be weaker than the bare coupling. It is just this running of the charge which leads to problems such as the Landau pole when attempts are made to take the theory's ultraviolet cutoff to infinity, and have lead to the suspicion that QED and other non-asymptotically free theories are trivial. Corrections to the photon propagator are therefore vital to any consideration of the triviality of QED. Any approximation that ignores vacuum

polarisation graphs is almost certain to find a non-trivial continuum limit for QED, while with such graphs present it is possible for the physical α to be zero.

The self-consistency relations of fig. 1 generate all one-loop diagrams. At the two-loop level they differ from the true Schwinger–Dyson equations because the bare fermion–photon vertex is used throughout. To minimise the effect of this approximation I use the Landau gauge, because in this gauge the order α contribution to the vertex vanishes. Euclidean momenta are used throughout.

The fermion propagator has the form

$$1/\left(iF(p^2)p^\mu\gamma_\mu + \Sigma(p^2)\right) \tag{2.1}$$

and the photon propagator

$$\frac{4\pi A(p^2)}{p^2}. \tag{2.2}$$

The photon and fermion renormalisation factors are related to A and F by

$$Z_3 = A(0)/\alpha_0, \qquad Z_2 = 1/F(0). \tag{2.3}$$

Because the bare vertex is always used, the vertex renormalisation factor $Z_1 = 1$.

The resulting integral equations for the fermion propagator are

$$\Sigma(p^2) = m_0 + \int_0^{\Lambda^2} \frac{k^2\,\mathrm{d}k^2}{4\pi}\,\frac{\Sigma(k^2)}{D(k^2)} \int_0^{\pi} \frac{\mathrm{d}\theta}{\pi} 2\sin^2\theta \frac{3A(q^2)}{q^2} \tag{2.4}$$

and

$$F(p^2) = 1 + \int_0^{\Lambda^2} \frac{k^2\,\mathrm{d}k^2}{4\pi}\,\frac{F(k^2)}{D(k^2)} \int_0^{\pi} \frac{\mathrm{d}\theta}{\pi} 2\sin^2\theta \frac{kA(q^2)}{q^4 p}\{3q^2\cos\theta - 2kp\sin^2\theta\}, \tag{2.5}$$

where $D(k^2) \equiv k^2F^2(k^2) + \Sigma^2(k^2)$ and $q^2 \equiv (k-p)^2 = k^2 + p^2 - 2kp\cos\theta$, the photon virtuality. If A is constant (the quenched case), the integrals over θ can be done analytically and the equation for F reduces to $F(p^2) = 1$ and eq. (2.4) reduces to Miransky's equation [1] for Σ.

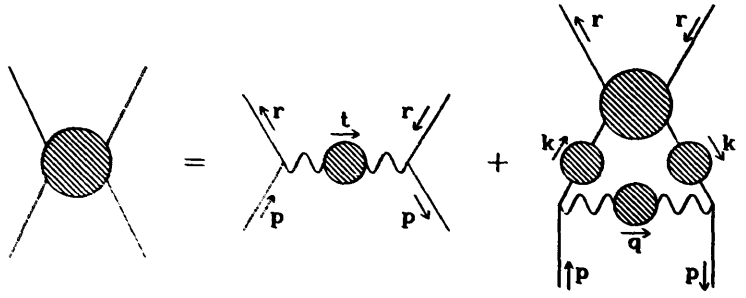

Fig. 2. The Feynman diagrams that lead to the Schwinger–Dyson equations for the fermion–anti-fermion scattering amplitude in the ladder approximation.

The equation for the photon propagator is

$$\frac{1}{A(p^2)} = \frac{1}{\alpha_0} - \frac{4}{3}N_f\int_0^{\Lambda^2}\frac{k^2\,dk^2}{4\pi}\int_0^{\pi}\frac{d\theta}{\pi}2\sin^2\theta\frac{F(q_+^2)}{D(q_+^2)}\frac{F(q_-^2)}{D(q_-^2)}\left\{\frac{k^2}{p^2}(8\cos^2\theta-2)-\tfrac{3}{2}\right\}, \tag{2.6}$$

where $q_\pm^2 \equiv (k \pm \frac{1}{2}p)^2 = k^2 + \frac{1}{4}p^2 \pm kp\cos\theta$, the virtualities of the fermion and anti-fermion.

It is also useful to write down the integral equations for the scalar and pseudo-scalar scattering amplitudes, shown in fig. 2. The case I consider is that of a fermion and anti-fermion of momentum p and $-p$ scattering to momentum r and $-r$. I average over the angles between initial and final momenta, which gives an amplitude depending on p^2 and r^2,

$$S_5(p^2,r^2) = \int_0^{\pi}\frac{d\theta}{\pi}2\sin^2\theta\frac{3\pi A(t^2)}{t^2} + \int_0^{\Lambda^2}\frac{k^2\,dk^2}{4\pi}\frac{S_5(k^2,r^2)}{D(k^2)}\int_0^{\pi}\frac{d\theta}{\pi}2\sin^2\theta\frac{3A(q^2)}{q^2}, \tag{2.7}$$

$$S_1(p^2,r^2) = \int_0^{\pi}\frac{d\theta}{\pi}2\sin^2\theta\frac{3\pi A(t^2)}{t^2} + \int_0^{\Lambda^2}\frac{k^2\,dk^2}{4\pi}S_1(k^2,r^2)\frac{k^2F^2(k^2)-\Sigma^2(k^2)}{D^2(k^2)}\int_0^{\pi}\frac{d\theta}{\pi}2\sin^2\theta\frac{3A(q^2)}{q^2}, \tag{2.8}$$

where S_5 and S_1 are the pseudo-scalar and scalar scattering amplitudes respectively, $t^2 \equiv p^2 + r^2 - 2pr\cos\theta$ and $q^2 \equiv p^2 + k^2 - 2pk\cos\theta$. Note that the integral

equations for the scattering amplitudes are linear, unlike those for the propagators.

I solve this system of integral equations on the computer by representing the unknown functions $A(p^2)$, $F(p^2)$ and $\Sigma(p^2)$ as Chebyshev polynomials in the variable $\log(p^2)$, with p ranging between the ultraviolet cut-off Λ and an infrared cut-off much smaller than the renormalised fermion mass. ($\log(p^2)$ is a good choice of variable because the functions are smooth when plotted against $\log(p^2)$). Away from the phase transition the propagators are well represented by 20 terms of the series. Near the phase transition (when correlation lengths are large) I use 30 terms. This is enough to solve the equations for correlation lengths of up to 10^{12} times the cut-off.

3. Propagators, scaling and critical behaviour

The solution of the Schwinger–Dyson equations gives the photon and fermion propagators, from which we can understand much of the physics of the system. First I look for scaling at constant renormalised coupling. The renormalised mass and coupling are defined at zero momentum by

$$m_r \equiv \Sigma(0)/F(0), \qquad \alpha_r \equiv A(0)/F^2(0). \qquad (3.1), (3.2)$$

If scaling holds the propagators should be functions of p^2/m_r^2 at a given value of the renormalised coupling α_r.

This is tested in figs. 3 and 4 which show scaling plots of the photon and fermion propagators. The propagators are shown for $\alpha_r = 0.5$ and for three very different values of the renormalised mass m_r. ($m_r/\Lambda = 10^{-1}$, 10^{-3} and 10^{-4}). As always N_f, the number of flavours, is 1. When plotted against p/m_r we see immediately that scaling is very good in both cases.

We can also use the solutions of the Schwinger–Dyson equations to get some information on the error introduced by the truncation. Fig. 5 shows F, the fermion wave-function renormalisation. Because the truncated Schwinger–Dyson equations of sect. 2 assume that the dressed and bare vertices are equal, the deviation of $F(p^2)$ from $F(0)$ is a measure of the violation of the Ward identity $Z_1 = Z_2$. This deviation is not large (on the order of 10% to 20% for most values of α_r). The violation of the Ward identity would be far larger in any other gauge. In the Landau gauge the deviation is of order α_r^2, in other gauges it is of order α_r. (The effects of using other gauges are discussed in ref. [9].)

Fig. 6 shows the dependence of the chiral condensate $\langle\bar{\psi}\psi\rangle$ on the bare couplings α_0 and m_0. When α_0 is small $\langle\bar{\psi}\psi\rangle$ vanishes as $m_0 \to 0$, as chiral symmetry requires. There is however clearly a second-order phase transition, with

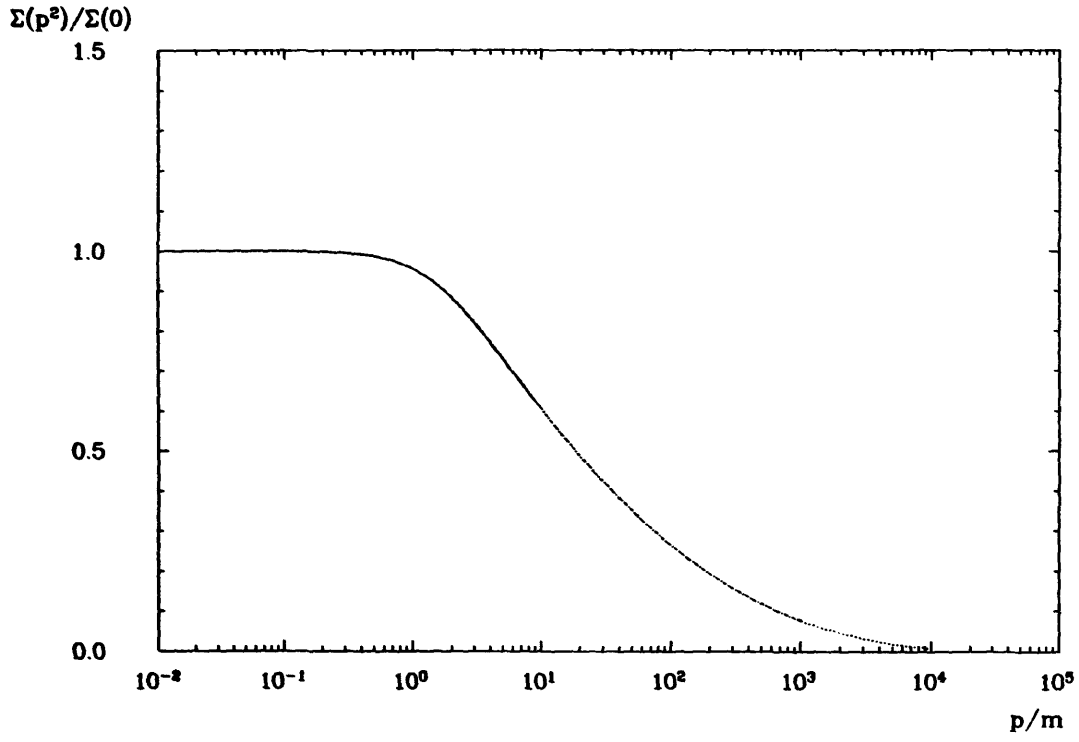

Fig. 3. Σ, the scalar part of the fermion propagator, for $\alpha_r = 0.5$ and three different values of the cutoff. (The solid line is $m_r/\Lambda = 10^{-1}$, the dashed line $m_r/\Lambda = 10^{-3}$ and the dotted line $m_r/\Lambda = 10^{-4}$.) The agreement of the curves shows that scaling holds.

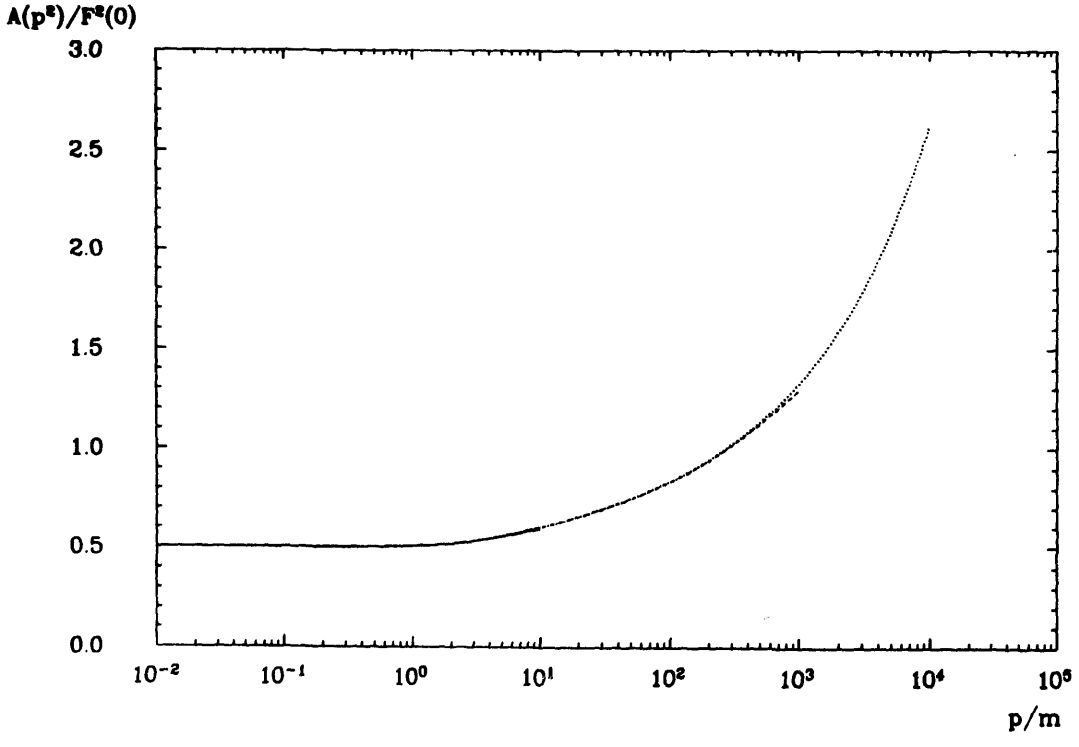

Fig. 4. The photon propagator as a function of a momentum for $\alpha_r = 0.5$ and three different values of the cutoff. (The solid line is $m_r/\Lambda = 10^{-1}$, the dashed line $m_r/\Lambda = 10^{-3}$ and the dotted line $m_r/\Lambda = 10^{-4}$.) The agreement between the curves shows that scaling holds.

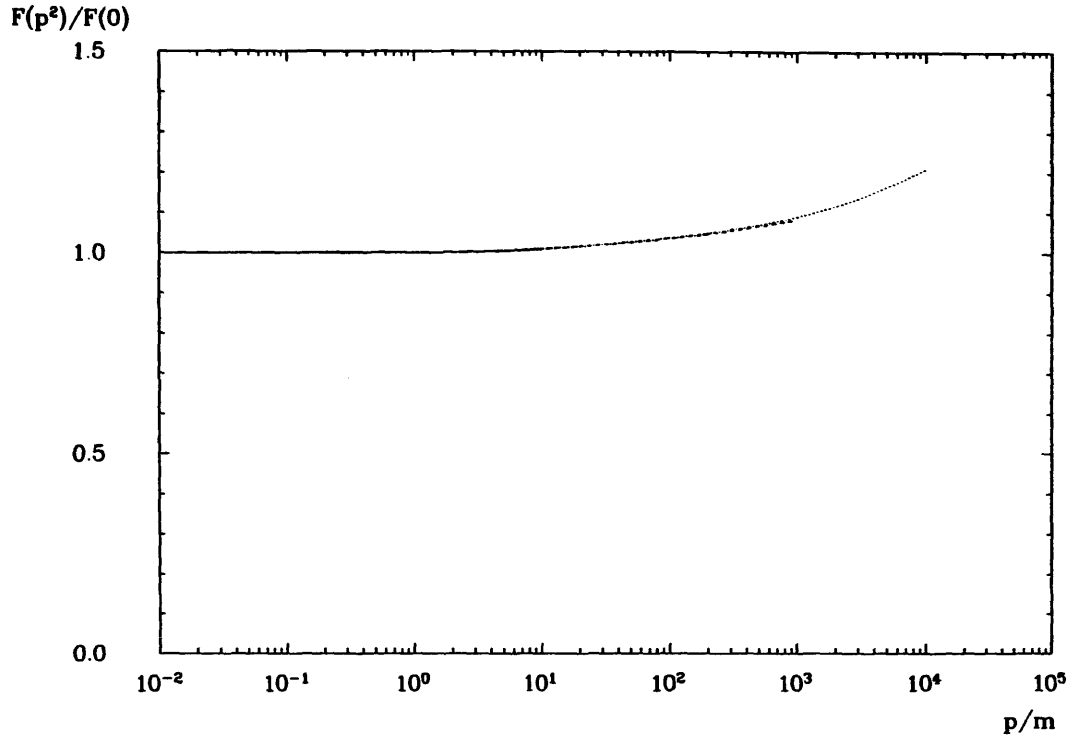

Fig. 5. The fermion wave-function renormalisation F as a function of momentum. The deviation of F from a constant value is a measure of the error introduced by using the bare vertex instead of the dressed in the Schwinger–Dyson equations ($\alpha_r = 0.5$, $m_r/\Lambda = 10^{-1}$, 10^{-3} and 10^{-4}).

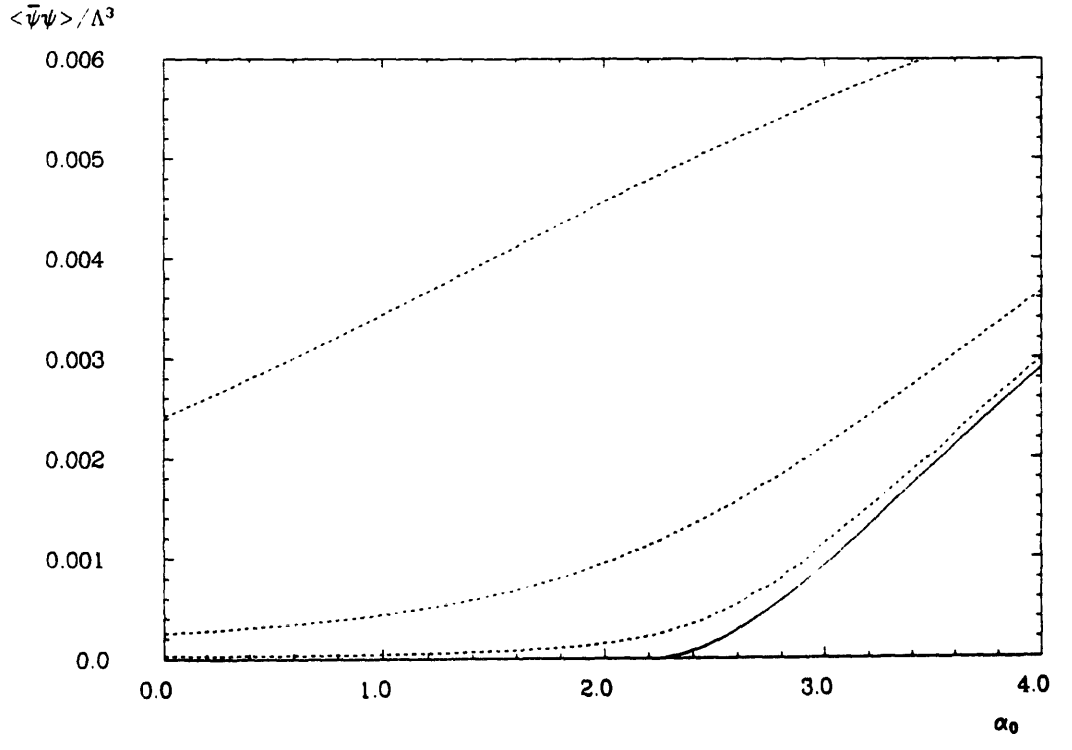

Fig. 6. A graph showing the chiral condensate $\langle\bar{\psi}\psi\rangle/\Lambda^3$ as a function of bare coupling α_0. The dashed lines show the results for bare masses $m_0/\Lambda = 10^{-n}$, $n = 1, 2, 3$. The solid line is the result for $m_0 = 0$. The chiral phase transition is at $\alpha_0 = 2.25$.

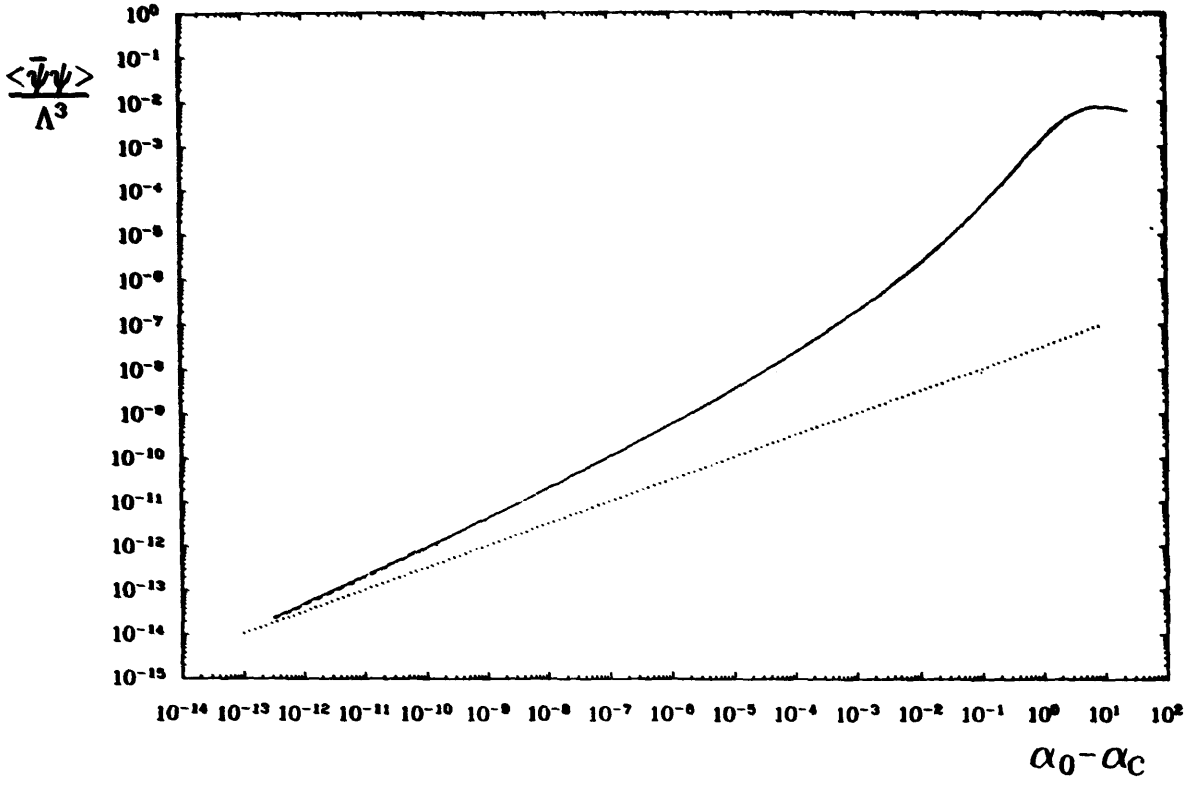

Fig. 7. A log–log plot of the chiral condensate $\langle\bar{\psi}\psi\rangle/\Lambda^3$ against $\alpha_0 - \alpha_c$ for $m_0 = 0$. The solid curve is the result of solving the Schwinger–Dyson equations, the dotted straight line is proportional to $(\alpha_0 - \alpha_c)^{1/2}$ (pure mean-field behaviour).

chiral symmetry spontaneously broken in the strongly coupled phase. The critical coupling for one flavour is $\alpha_c = 2.25$ (to be compared with $\pi/3$ for the quenched case). When chiral symmetry is broken the Schwinger–Dyson equations can be solved even at $m_0 = 0$, the limitation is the fermion correlation length, which must be less than about $10^{12}/\Lambda$. (On the lattice, results at $m_0 = 0$ have to be obtained by extrapolation from finite m_0.) Miransky [1] finds that the $m_0 = 0$ values of $\langle\bar{\psi}\psi\rangle$ and m_r exhibit an essential singularity, both vanishing faster than any power of $\alpha - \alpha_c$ as the critical coupling is approached from above. This happens only in the quenched case. The behaviour found here with fermion loops included looks like a power law. Other authors who have investigated the effect of modifying the photon propagator [10, 11] also find a power law behaviour for $N_f \neq 0$. Fig. 7 shows a log–log plot of $\langle\bar{\psi}\psi\rangle$ (for zero bare mass) against $\alpha - \alpha_c$. The approach to the asymptotic slope is clearly very slow. Unless you look very close to the critical point you will overestimate the critical exponents (as I initially did). The asymptotic slope is probably $\frac{1}{2}$, corresponding to mean field critical exponents. With more than one flavour the slope approaches the mean field value more rapidly. Renormalised mass shows a critical behaviour very like that of $\langle\bar{\psi}\psi\rangle$, with a slow approach to an asymptotic slope near $\frac{1}{2}$.

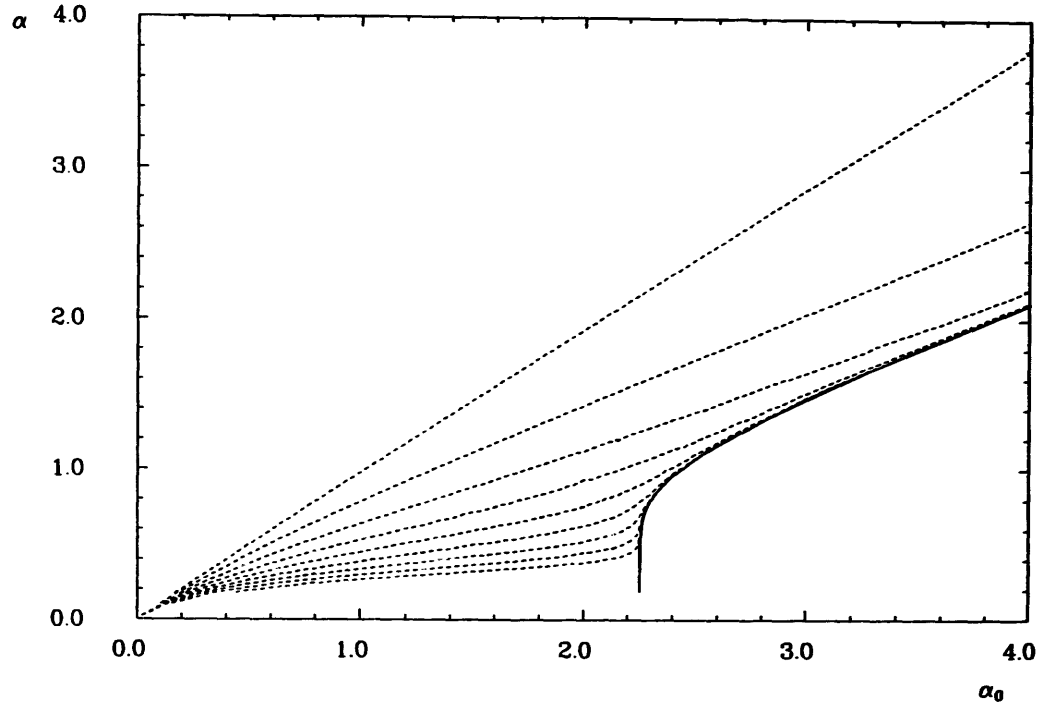

Fig. 8. A graph showing the renormalised coupling α_r as a function of bare coupling α_0. The dashed lines show the results for bare masses $m_0/\Lambda = 10^{-n}$, $n = 0, 8$. The solid line is the result for $m_0 = 0$. In the chirally symmetric phase, $\alpha_0 < 2.25$, $\alpha_r \to 0$ as $m_0 \to 0$.

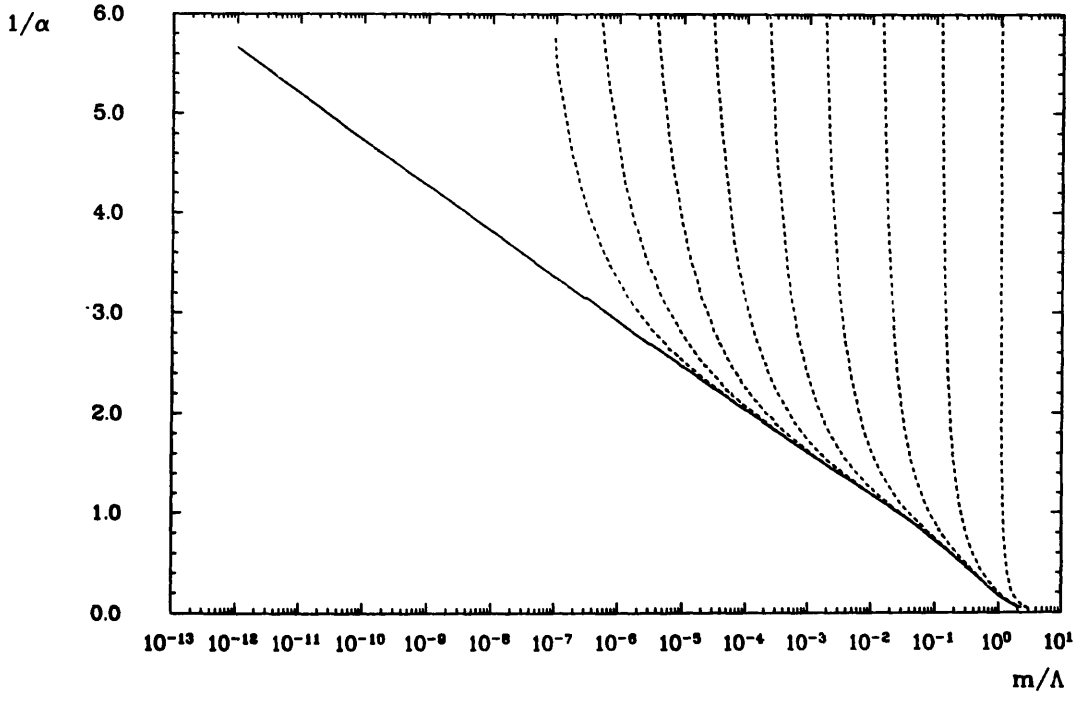

Fig. 9. A graph comparing the renormalised coupling α_r and the renormalised mass m_r. The dashed lines show the results for bare masses $m_0/\Lambda = 10^{-n}$, $n = 0, 8$. The solid line is the result for $m_0 = 0$. Note that for a general value of α_r the minimum possible value of m_r/Λ is always finite. Assuming that the straight line behaviour of the $m_0 = 0$ curve continues (as expected from the renormalisation group) an infinite fermion correlation length is only possible at $\alpha_r = 0$.

Fig. 8 shows α_r. The renormalised coupling vanishes as α_0 approaches α_c, although this vanishing is only logarithmic. The critical behaviour of α_r is revealed more clearly in fig. 9 which shows a plot of $1/\alpha_r$ against m_r. The straight line behaviour at $m_0 = 0$ shows that $\alpha_r \propto 1/\log(m_r)$, which of course vanishes as $m_r \to 0$. (This is exactly the behavior that would be expected on renormalisation group grounds.) This plot also shows that for any given α_r there is a minimum value of m_r. Only at $\alpha_r = 0$ is the fermion correlation length infinite. This tells us that the continuum limit of QED does not involve photons interacting with charged fermions. The behaviour $\alpha_r \propto 1/\log(m_r)$ is exactly the behaviour that would be expected on renormalisation group grounds.

4. Renormalisation group flow for pure QED

To truly understand the structure of this model we need to know the renormalisation flow. Fig. 10 shows lines of constant renormalised α_r in the bare coupling plane. All the trajectories end at $m_0 = 0$ in the phase with broken chiral symmetry (where the fermion correlation length and mass are finite).

The pattern of the flow is easy to explain quantitatively. At very large bare masses fermion loops are suppressed, and the renormalised and bare couplings are

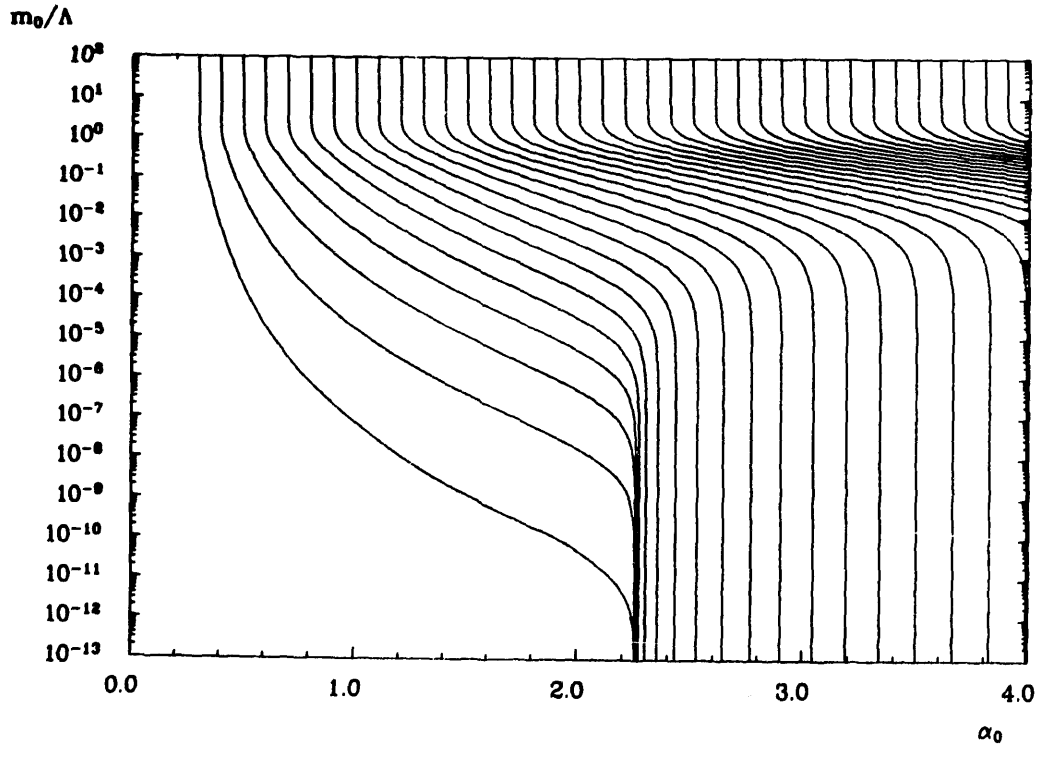

Fig. 10. The renormalised trajectories defined by keeping α_r constant. All the trajectories with finite α_r end at $m_0 = 0$, $\alpha_0 > \alpha_c$ (i.e. in the phase where chiral symmetry is broken, and the fermion correlation length is finite).

the same. This gives the vertical portion of the trajectory at the top of fig. 10. As the bare mass is reduced fermion loops cause more efficient shielding of the charge and the renormalised α is less than the bare, giving a sloping trajectory at intermediate values of m_0. This running of α eventually stops at large α_0 because the trajectory moves into the phase where the chiral symmetry is broken. There the mass of the fermion comes mainly from the spontaneous breaking of chiral symmetry, and reducing m_0 no longer leads to a significant reduction in the fermion mass or improvement in the shielding. This is the reason for the vertical portion of the renormalisation group trajectory at small m_0.

Note that despite the existence of a phase transition a decrease in m_0 always requires an increase in α_0 to keep α_r constant. In other words the β-function defined by keeping α_r constant never becomes negative, despite the existence of a second-order phase transition.

The lines of constant α_r are however not the entire story. As shown in sect. 3 the photon and fermion propagators scale on these trajectories. Fig. 11 shows the

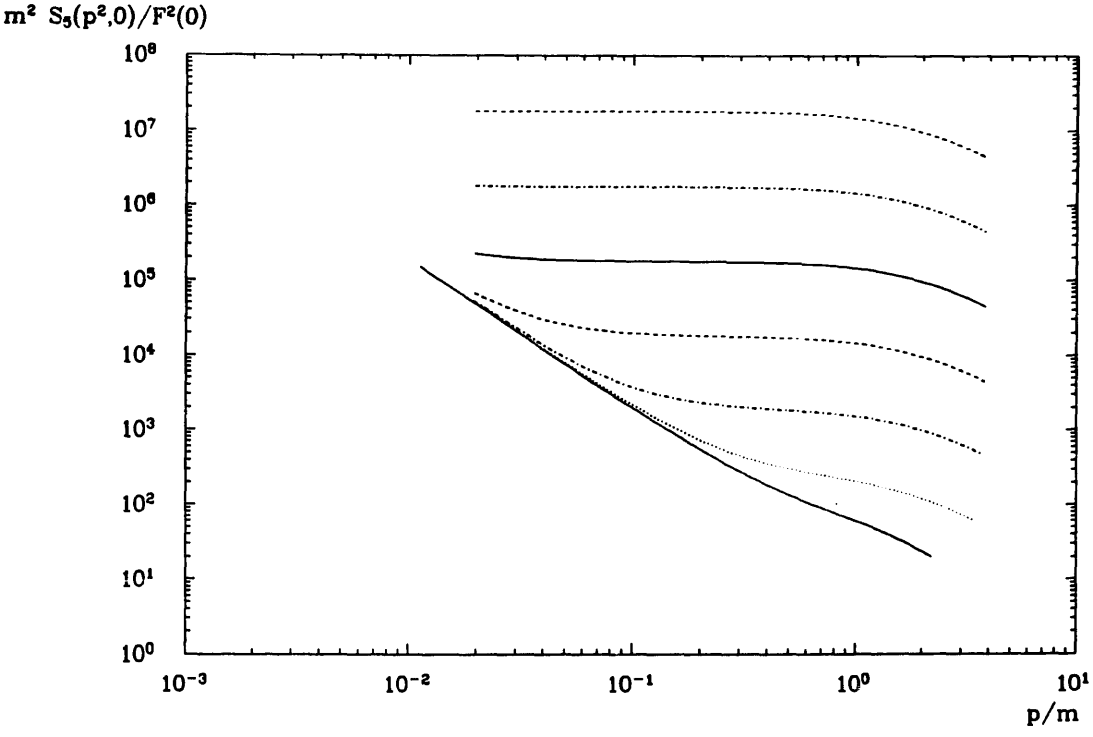

Fig. 11. The pseudo-scalar fermion–antifermion scattering amplitude at various points on a constant α_r trajectory. ($\alpha_r = 2.0$, $m_0/\Lambda = 10^{-n}$, $n = 1, 7$). The lowest curve is for $m_0/\Lambda = 10^{-1}$, the highest $m_0/\Lambda = 10^{-7}$. At low momenta the scattering amplitude is dominated by the exchange of a single photon, leading to a $1/p^2$ momentum dependence. At large momenta there is also another contribution which increases as the bare mass decreases. At $m_0 = 0$ this contribution is infinite. This new contribution is due to the formation of a Goldstone boson in the s-channel, and does not scale in the same way as the rest of the amplitude. This failure to scale is evidence that a further operator is needed.

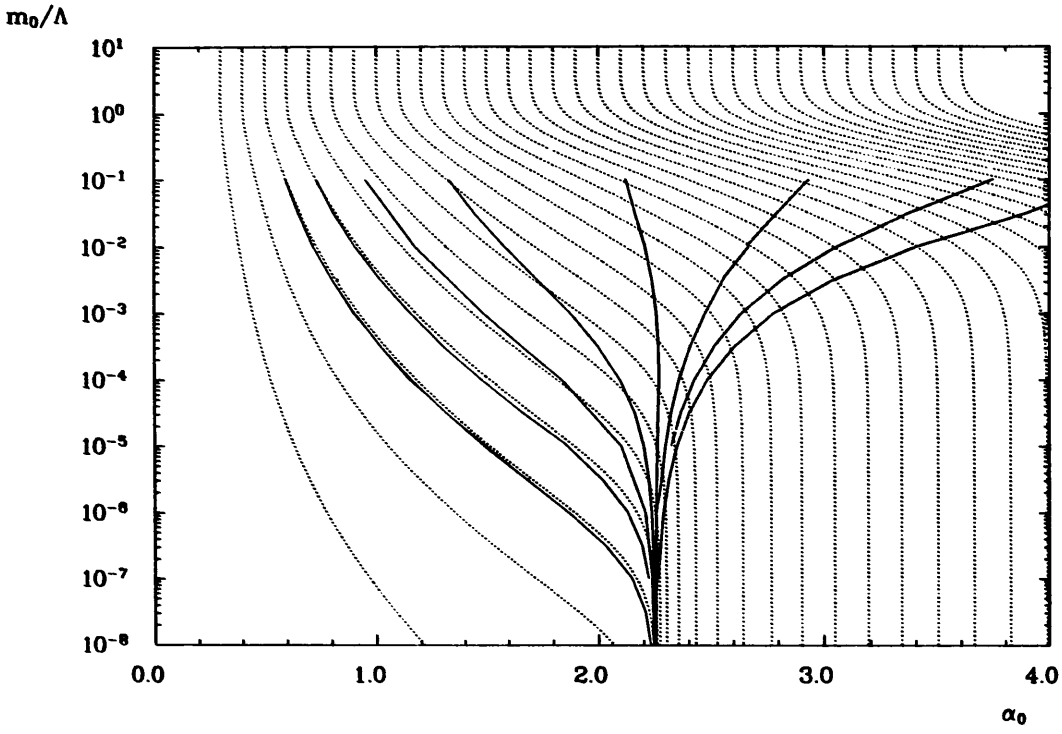

Fig. 12. The renormalised trajectories defined by keeping the pseudo-scalar scattering amplitude $m_r^2 S_5(m_r^2, 0)/F^2(0)$ constant. All the trajectories end in the critical point $m_0 = 0$, $\alpha_0 = \alpha_c$. The dotted lines show lines of constant α_r for comparison. The two ways of defining renormalisation group trajectories agree well at low α_0 but diverge for strong couplings.

pseudo-scalar fermion anti-fermion scattering amplitude at various points on a single curve of constant α_r ($\alpha_r = 2$). At low momenta the scattering amplitude is dominated by the exchange of a single photon, leading to an amplitude of $3\pi\alpha_r/p^2$, which is clearly constant along a constant α_r trajectory. At large momenta there is also another contribution which is much flatter, and which increases as the bare mass decreases. This large p contribution grows like $1/m_0$ and at $m_0 = 0$ it becomes infinite. This contribution to the scattering comes from the fermion and anti-fermion binding together to form a pseudo-scalar bound state, the Goldstone boson associated with the breaking of chiral symmetry. The dependence on the bare mass comes about because the Goldstone boson's mass decreases as the bare mass decreases, eventually becoming massless at $m_0 = 0$.

In addition to the lines of constant α_r we can consider lines of constant scattering amplitude. Fig. 12 shows the trajectories found by keeping the renormalised pseudo-scalar scattering amplitude $m_r^2 S_5(m_r^2, 0)/F^2(0)$ constant and compares them with the lines of constant α_r. (The scattering amplitude is divided by $F^2(0)$ because $Z_2 = 1/F(0)$, eq. (2.3)). In the symmetric phase the two sets of trajectories agree very well, showing a scattering amplitude that is a function of α_r, as would be naively expected. However in the broken phase the two sets of

trajectories are completely different. The lines of constant scattering all flow into the critical point at $\alpha = \alpha_c$, $m_0 = 0$. It is clear on the following grounds that the pseudo-scalar flows cannot follow the pattern found for the lines of constant α_r, and must have a flow similar to that found, all ending in the critical point. Lines of finite constant scattering amplitude can never reach the $m_0 = 0$ line in the broken symmetry phase, because there the pseudo-scalar scattering amplitude is infinite, due to the contribution of the massless Goldstone boson. Nor can they reach the $m_0 = 0$ line in the symmetric phase because there $\alpha_r \to 0$ leading to vanishing scattering amplitude.

Lines of constant scalar scattering amplitude (see fig. 13) show a flow pattern that shares some of the features of the pseudo-scalar case and some of the features of the constant α_r case. Again the flows follow lines of constant α_r in the chirally symmetric phase, but deviate in the broken phase. However, lines of constant S_1 can end on the $m_0 = 0$ line in the broken phase (because there is no massless scalar bound state). The lines corresponding to small scattering amplitudes end in the critical point.

The ratios of the meson mass to the fermion mass should flow in the same way as the scattering amplitude in the same channel. The fact that scalar trajectories can end on the axis at places other than the critical point simply means that in the

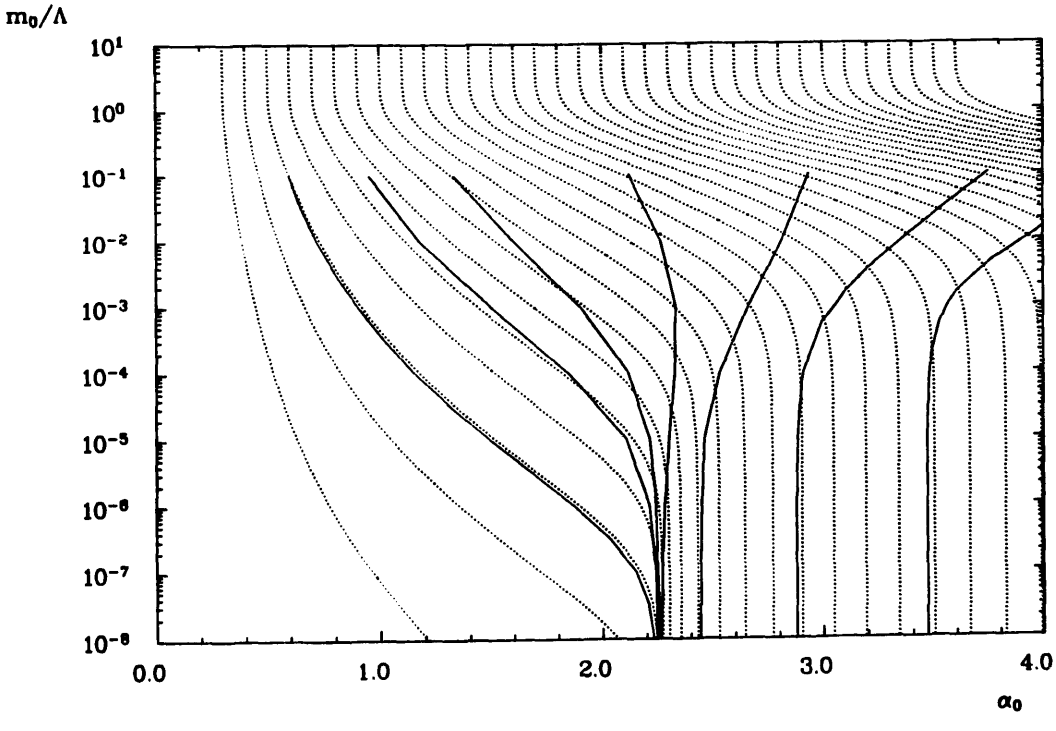

Fig. 13. The renormalised trajectories defined by keeping the scalar scattering amplitude $m_r^2 S_1(m_r^2, 0)/F^2(0)$ constant. The dotted lines show lines of constant α_r for comparison. Compare this graph with fig. 12, the pseudo-scalar case.

broken phase the ratio of fermion mass to scalar meson mass has a finite limit as $m_0 \to 0$ (while the pseudo-scalar meson is naturally massless).

5. Renormalisation flow with a four-Fermi coupling

It is clear from the mismatch between the lines of constant α_r and constant scattering amplitude that only by adding another operator to our action can the physics be kept constant while changing the cutoff. In company with a number of other authors [5,8] I consider the effect of adding a four-Fermi interaction to the action.

A chirally invariant four-Fermi interaction term is

$$\frac{G_0}{2}((\bar{\psi}\psi)(\bar{\psi}\psi) - (\bar{\psi}\gamma_5\psi)(\bar{\psi}\gamma_5\psi)). \tag{5.1}$$

(This is the interaction of the Nambu–Jona-Lasinio model [7].) The changed

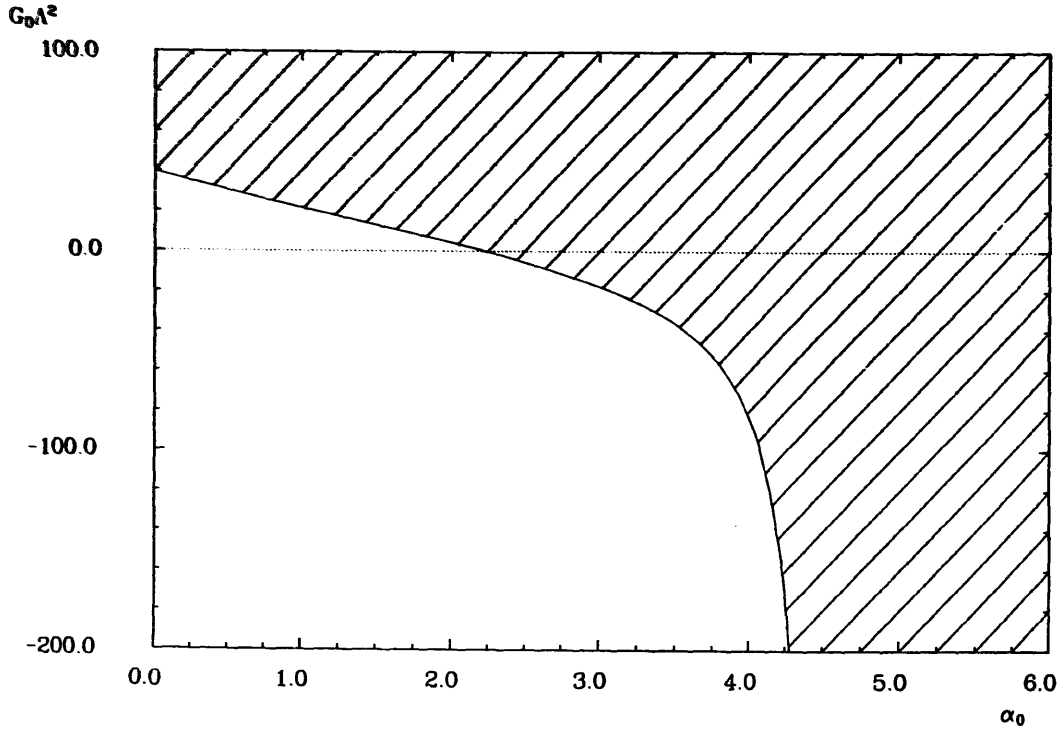

Fig. 14. The phase diagram when a four-Fermi interaction is included. Chiral symmetry is broken at high G_0 and at high α_0.

ladder approximation equations the Σ and S_5 are

$$\Sigma(p^2) = m_0 + \int_0^{\Lambda^2} \frac{k^2\,dk^2}{4\pi} \frac{\Sigma(k^2)}{D(k^2)} \int_0^{\pi} \frac{d\theta}{\pi} 2\sin^2\theta \frac{3A(q^2)}{q^2} + \frac{G_0}{\pi} \int_0^{\Lambda^2} \frac{k^2\,dk^2}{4\pi} \frac{\Sigma(k^2)}{D(k^2)}, \tag{5.2}$$

$$S_5(p^2, r^2) = \int_0^{\pi} \frac{d\theta}{\pi} 2\sin^2\theta \frac{3\pi A(t^2)}{t^2} + G_0 + \int_0^{\Lambda^2} \frac{k^2\,dk^2}{4\pi} \frac{S_5(k^2, r^2)}{D(k^2)}$$

$$\times \int_0^{\pi} \frac{d\theta}{\pi} 2\sin^2\theta \frac{3A(q^2)}{q^2} + \frac{G_0}{\pi} \int_0^{\Lambda^2} \frac{k^2\,dk^2}{4\pi} \frac{S_5(k^2, r^2)}{D(k^2)}. \tag{5.3}$$

The momenta have the same definitions as in eqs. (2.4) and (2.7). The equations for F and A are unchanged (eqs. (2.5) and (2.6)). (Note that in this new equation for Σ, the quantity that G_0 couples to is $\langle\bar{\psi}\psi\rangle$. This suggests that the effects of the new term in the lagrangian will become important when the chiral symmetry is broken and $\langle\bar{\psi}\psi\rangle$ acquires a vacuum expectation value.)

The phase diagram with the new interaction is shown in fig. 14. At $\alpha_0 = 0$ the theory is the Nambu–Jona-Lasinio model [7] with a chiral phase transition at $G_0\Lambda^2 = 4\pi^2$. The Monte Carlo simulations of ref. [5] show just such a phase

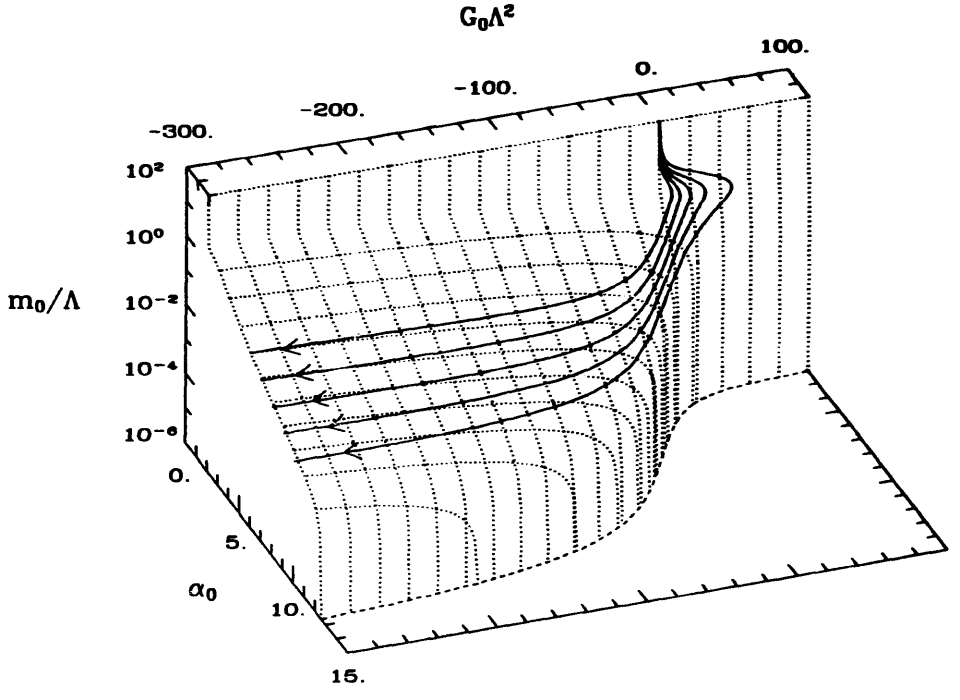

Fig. 15. The surface $\alpha_r = 2$ and paths within this surface that keep both α_r and the pseudo-scalar scattering amplitude constant. The lines of constant physics begin at $\alpha_0 = \alpha_r$, $m_0 = \infty$ and end at $G_0 = -\infty$.

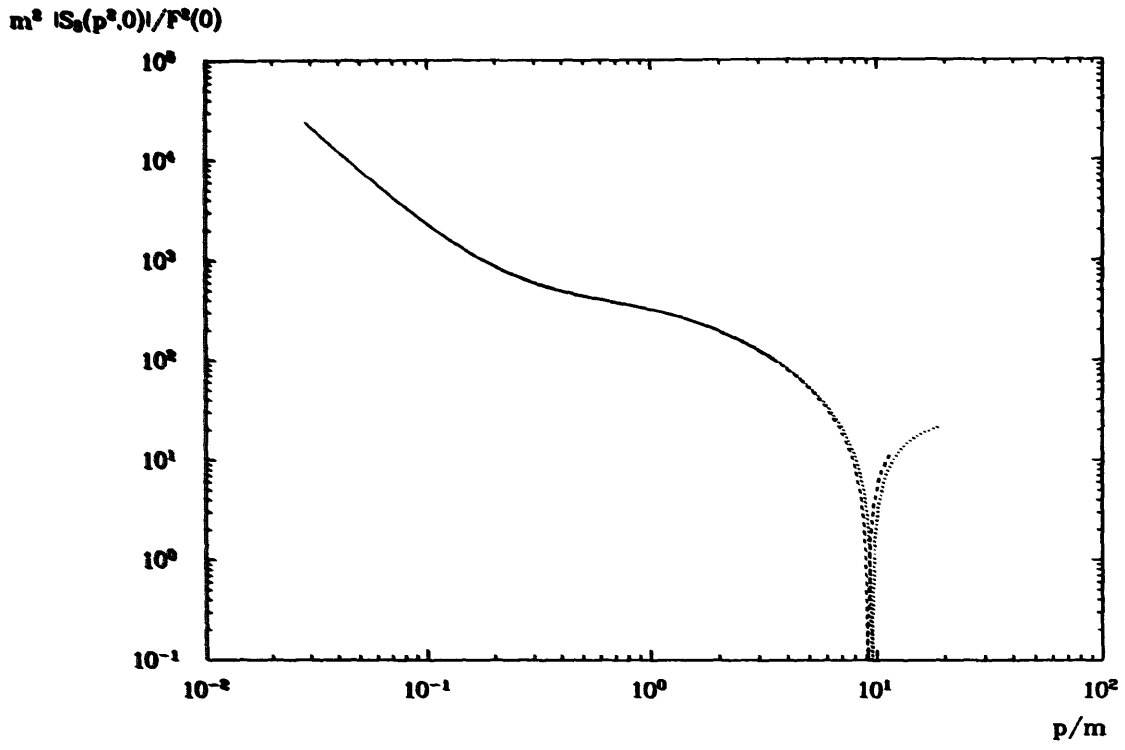

Fig. 16. The pseudo-scalar fermion–antifermion scattering amplitude at various points on one of the trajectories of fig. 15. With two couplings, α_0 and G_0, the scattering amplitude now scales. Contrast this with the situation in figure 11, with no four-Fermi interaction.

diagram when both interaction terms are present. The shape of the phase boundary is similar to that found in the quenched planar approximation [8].

The fermion and photon propagators scale as before. Now the extra coupling allows us to define renormalisation group trajectories which are true lines of constant physics. The trajectories shown in fig. 15 keep both the renormalised charge α_r and the pseudo-scalar scattering amplitude $m_r^2 S_5(m_r^2, 0)/F^2(0)$ constant. Fig. 16 shows that fixing these two quantities is enough to insure that the scattering amplitude at all momenta scales just as well as the propagators now that G_0 has been introduced. Contrast this with the situation shown in fig. 11 for pure QED.

The trajectories of constant physics move through a three-dimensional space defined by α_0, G_0 and m_0. In this three-dimensional space the surfaces of constant α_r form two-dimensional sheets. These surfaces are bounded on the left (low α_0) side by the line $\alpha_0 = \alpha_r$, $m_0 = \infty$ and on the right by $m_0 = 0$. The lines of constant α_r shown in sect. 4 (for QED without a four-Fermi interaction) show the section through these sheets of constant α_r at $G_0 = 0$, which is typical of slices at constant G_0. Fig. 15 shows a surface of constant α_r ($\alpha_r = 2.0$). This constant α_r surface never touches the phase boundary of fig. 14.

The curves shown by the solid lines in fig. 15 show renormalisation group flows with α_r and the scattering amplitude kept constant. Trajectories with finite

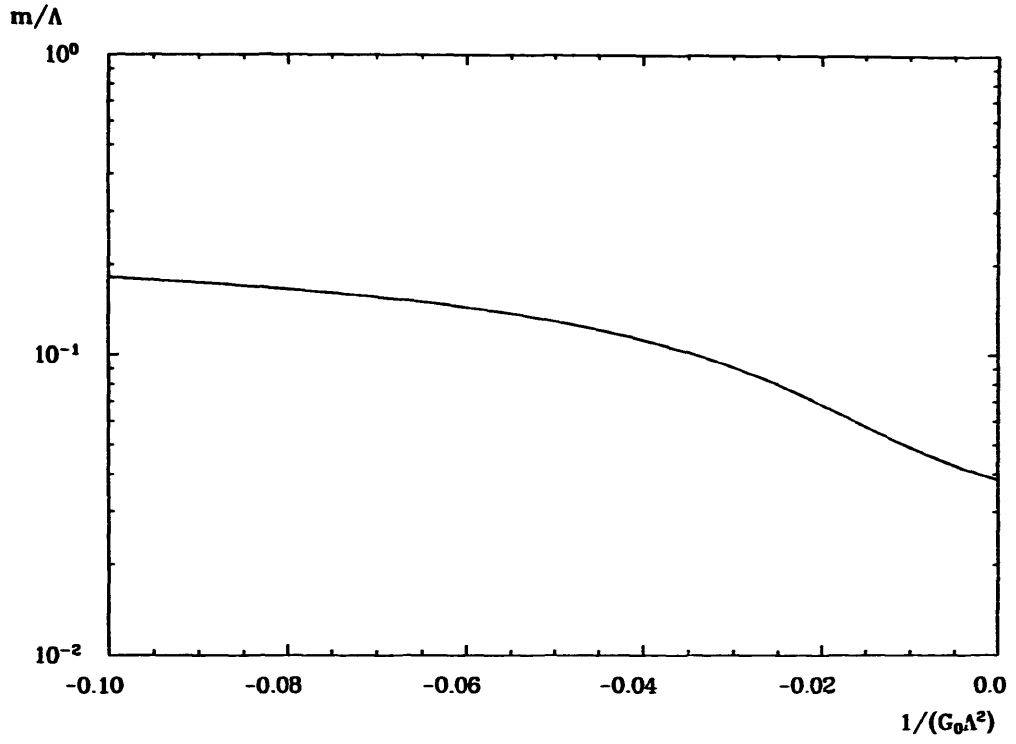

Fig. 17. The variation of renormalised fermion mass on the $\alpha_r = 2$ renormalisation group trajectory with infinite pseudo-scalar scattering amplitude (which has $m_0 = 0$). The limit of m_r as $G_0 \to -\infty$ is finite. Even with a four-Fermi interaction added to the lagrangian it is impossible to have an infinite fermion correlation length for non-zero α_r.

scattering amplitude begin at $m_0 = \infty$, $\alpha_0 = \alpha_r$ and move in the direction of increased α_0. (Flow is defined as moving in the direction of increased correlation length.) The trajectories end at $G_0 = -\infty$, with various values of α_0. The trajectories show no sign of meeting in some common ultraviolet fixed point. When the paths get to $G_0 = -\infty$ the fermion correlation length still has a finite value. The trajectory with $S_5 = \infty$ moves along the $m_0 = 0$ edge of the constant α_r sheet, beginning at $G_0 = +\infty$ and ending at $G_0 = -\infty$. (The path of this limiting trajectory in the α_0–G_0 plane is the dashed line of fig. 15.) Even this limiting trajectory always has a finite correlation length. This is illustrated in fig. 17, which shows the fermion mass along the chiral ($m_0 = 0$) trajectory. (The other flow lines, with $m_0 \neq 0$ have larger renormalised fermion masses.) It is natural that the fermion correlation length is always finite within a constant α_r surface, because these surfaces never touch the phase boundary, which is where the fermion correlation length is infinite.

The finiteness of the fermion correlation length means that adding the four-Fermi interaction has not changed the conclusion that only at $\alpha_r = 0$ is there a continuum limit with a fermion present. (The limiting trajectory, at $m_0 = 0$, which has an infinite pseudo-scalar scattering amplitude, will of course have a massless

Goldstone boson, but this will be electrically neutral, and so not interact with the photon.)

6. Conclusion

In this paper I have looked at the renormalisation group flow for a set of truncated Schwinger–Dyson equations which include vacuum polarisation effects, considering the theory with and without a four-Fermi interaction term.

Consider first the behaviour found in pure QED, as discussed in sect. 4. The lines of constant renormalised coupling α_r that result from the truncated equations correspond to a renormalised coupling at the phase transition of 0. If the renormalised coupling is finite the fermion correlation length cannot be taken to infinity, but has some finite maximum, as can be seen clearly in fig. 9. The explanation for this fact is quite simple. The lighter a fermion is, the better it is at shielding charge. In the chirally symmetric phase decreasing the bare mass of the fermion decreases its renormalised mass, and the bare coupling α_0 must be increased to compensate for the improved shielding. However, once the flow has reached the broken symmetry phase, the renormalised mass of the fermion is mainly due to symmetry breaking and only weakly dependent on the bare mass. A decrease in the bare mass no longer causes any great improvement in shielding, and so no change in α_0 is needed to keep α_r constant. The fact that the behaviour found in sect. 4 is readily comprehensible suggests that the full theory will behave in the same way.

In the broken phase the scalar and pseudo-scalar scattering amplitudes follow different flow patterns from those defined by keeping α_r constant, while in the symmetric all three flows agree. The fact that flows defined in different ways disagree in the broken phase is evidence that a new scale is introduced when the Goldstone boson forms. This is to be expected in the broken phase because the mass of the Goldstone boson has to vanish as $m_0 \to 0$, while the mass of the fermion will be finite in terms of the cutoff.

Many of the results from this analysis of the Schwinger–Dyson equations lend themselves to tests in Monte Carlo simulations of QED.

Lattice measurements of α_r could be compared with the flow patterns of fig. 10, or plotted against measurements of the fermion mass (as in fig. 9). Such comparisons would go a long way towards settling the nature of the phase transition, although the range of correlation lengths possible on the lattice is of course far smaller than the range considered in this paper.

The result that in pure QED the lines of constant scattering amplitude and the lines of constant α_r do not agree can be tested by measuring α_r from Wilson loops or from the photon propagator, and comparing these to mass ratios, in particular the pion to fermion mass ratio, which should behave like the pseudo-scalar

scattering flow. Similarly, lines of constant scalar meson to fermion mass ratio should look like the curves in fig. 12.

In sect. 5 I investigated the theory in the presence of a four-Fermi interaction. The largest fermion correlation lengths occur when G_0 is large and negative (i.e. repulsive), but even in this region it is not possible to have an infinite fermion correlation length and a finite α_r, i.e. a continuum limit involving photons interacting with charged fermions. It would be interesting to find out what happens on the lattice with negative G_0, and compare this with the results of sect. 5.

I would like to thank Gerrit Schierholz for various conversations during the progress of this work.

References

[1] V.A. Miransky, Nuovo Cimento 90A (1985) 149; Sov. Phys. JETP 61 (1985) 905;
P.I. Fomin, V.P. Gusynin, V.A. Miransky and Yu.A. Sitenko, Riv. Nuovo Cimento 6 (1983) 1
[2] K.I. Aoki, Kyoto preprint RIFP-758 (1988)
[3] J.B. Kogut, E. Dagotto and A. Kocic, Nucl. Phys. B317 (1989) 253, 271;
S. Hands, J.B. Kogut and E. Dagotto, Santa Barbara ITP preprint NSF-ITP-89-180 (1989)
[4] M. Göckeler, R. Horsley, E. Laermann, P. Rakow, G. Schierholz, R. Sommer and U.-J. Wiese, Nucl. Phys. B334 (1990) 527
[5] S.P. Booth, R.D. Kenway and B.J. Pendleton, Phys. Lett. B228 (1989) 115
[6] L.D. Landau and E.M. Lifshitz, Relativistic quantum theory (Pergamon, Oxford, 1974)
[7] Y. Nambu and G. Jona-Lasinio, Phys. Rev. 122 (1961) 345
[8] C.N. Leung, S.T. Love and W.A. Bardeen, Nucl. Phys. B273 (1986) 649
[9] T. Nonoyama and M. Tanabashi, Prog. Theor. Phys. 81 (1989) 209
[10] K. Kondo, Y. Kikukawa and H. Mino, Phys. Lett. B220 (1989) 270
[11] J. Olienses and P.W. Johnson, Argonne preprint ANL-HEP PR-88-45 (1988)